

Species-specific Inhibition of Porphobilinogen Synthase by 4-Oxosebacic Acid*

Received for publication, February 13, 2002, and in revised form, March 19, 2002
Published, JBC Papers in Press, March 21, 2002, DOI 10.1074/jbc.M201486200

Eileen K. Jaffe^{‡§}, Jukka Kervinen^{‡¶}, Jacob Martins[‡], Frédéric Stauffer^{||**}, Reinhard Neier^{||},
Alexander Wlodawer^{‡‡}, and Alexander Zdanov^{‡‡}

From the [‡]Institute for Cancer Research, Fox Chase Cancer Center, Philadelphia, Pennsylvania 19111, the ^{||}Department of Chemistry, University of Neuchâtel, Neuchâtel 2007, Switzerland, and the ^{‡‡}Macromolecular Crystallography Laboratory, NCI-Frederick, National Institutes of Health, Frederick, Maryland 21702

Porphobilinogen synthase (PBGS) catalyzes the condensation of two molecules of 5-aminolevulinic acid (ALA), an essential step in tetrapyrrole biosynthesis. 4-Oxosebacic acid (4-OSA) and 4,7-dioxosebacic acid (4,7-DOSA) are bisubstrate reaction intermediate analogs for PBGS. We show that 4-OSA is an active site-directed irreversible inhibitor for *Escherichia coli* PBGS, whereas human, pea, *Pseudomonas aeruginosa*, and *Bradyrhizobium japonicum* PBGS are insensitive to inhibition by 4-OSA. Some variants of human PBGS (engineered to resemble *E. coli* PBGS) have increased sensitivity to inactivation by 4-OSA, suggesting a structural basis for the specificity. The specificity of 4-OSA as a PBGS inhibitor is significantly narrower than that of 4,7-DOSA. Comparison of the crystal structures for *E. coli* PBGS inactivated by 4-OSA versus 4,7-DOSA shows significant variation in the half of the inhibitor that mimics the second substrate molecule (A-side ALA). Compensatory changes occur in the structure of the active site lid, which suggests that similar changes normally occur to accommodate numerous hybridization changes that must occur at C3 of A-side ALA during the PBGS-catalyzed reaction. A comparison of these with other PBGS structures identifies highly conserved active site water molecules, which are isolated from bulk solvent and implicated as proton acceptors in the PBGS-catalyzed reaction.

Porphobilinogen synthase (PBGS,¹ EC 4.2.1.24, also known as 5-aminolevulinic acid dehydratase) recently has emerged as a

viable enzyme target for the development of pharmaceuticals or agricultural agents. The PBGS protein, which is highly conserved in both sequence and structure (1), catalyzes an early essential step in the biosynthesis of the tetrapyrrole cofactors such as heme and chlorophyll (Fig. 1A). Despite the fact that much is known about the PBGS structure, the sequence of bond-making and bond-breaking events that follow formation of the ternary complex of PBGS with the two substrate molecules is the subject of active discussion (2–5). Based on an extensive phylogenetic variation in the number and kinds of metal ions used for catalytic and/or allosteric roles, it is possible that the order of chemical events in the enzyme-catalyzed reaction mechanism may not be phylogenetically conserved. In order to probe the mechanism, 4,7-dioxosebacic acid (4,7-DOSA) and 4-oxosebacic acid (4-OSA), illustrated in Fig. 1B, were designed and found to act as suicide substrates for *Escherichia coli* PBGS (6). These inhibitors mimic an addition product intermediate in which the first bond formed between the two 5-aminolevulinic acid (ALA) substrate molecules creates a carbinolamine that dehydrates to a Schiff base (6). More recently, a strong species-selective inhibition of PBGS by 4,7-DOSA has been correlated with an active site variation in metal ion usage (3). Here we have characterized a very different species selectivity for 4-OSA inhibition of PBGS and provide a 1.9-Å crystal structure of 4-OSA-inhibited *E. coli* PBGS. This structure was compared with an improved 1.7-Å crystal structure of *E. coli* PBGS inhibited by 4,7-DOSA and with analogous structures of these inhibitors bound to yeast PBGS (for which, however, there are no kinetic inhibition data) (5).

EXPERIMENTAL PROCEDURES

Materials—Most chemicals and buffers were obtained from Fisher or Sigma in the purest available form. 2-Mercaptoethanol (β ME) from Fluka (Buchs, Switzerland) was vacuum-distilled prior to use. 4-OSA and 4,7-DOSA were synthesized and tested (as described in Ref. 6). All of the PBGS enzymes used in this study were cloned and expressed in *E. coli*, and purification and detailed characterization has been described previously (7–12). Human PBGS was the C162A variant of the natural N59 isozyme, and it has kinetic properties closely resembling the wild type (13). Human PBGS mutants characterized with 4-OSA were N59/C162A/H131A/C223A (called MinusZnA) (13) and two new chimeric proteins (Hs Δ ALK and HsEclid) containing portions of the *E. coli* PBGS active site lid. The chimeric proteins were prepared from the plasmid encoding wild type human PBGS variant N59/C162A by the QuikChange method of mutagenesis. The sense strand primers were CCGTTCGGTATGCGCTAAGTCAGCATTAAGGCGACCGCCGCTGC for Hs Δ ALK and CCGTTCGGTGAAGCTGCTGGGTCAGCCTTAAGGCGACCGCAAAGCTATCAG for HsEclid.

Activity Assays for PBGS—The enzyme assay measures the formation of porphobilinogen from ALA. The assay conditions at optimal pH and with a full complement of required and allosteric metal ions in the standard 5-min assay procedure for each of the five PBGS were performed as described previously (3). Human mutants MinusZnA,

* This work was supported by Grants ES03654 (to E. K. J.) and CA06927 (to I. C. R.) from the NIEHS and NCI of the National Institutes of Health and by an appropriation from the Commonwealth of Pennsylvania. The costs of publication of this article were defrayed in part by the payment of page charges. This article must therefore be hereby marked "advertisement" in accordance with 18 U.S.C. Section 1734 solely to indicate this fact.

The atomic coordinates and structure factors (code 1L6S and 1L6Y) have been deposited in the Protein Data Bank, Research Collaboratory for Structural Bioinformatics, Rutgers University, New Brunswick, NJ (<http://www.rcsb.org/>).

§ To whom correspondence should be addressed: Inst. for Cancer Research, Fox Chase Cancer Center, 7701 Burholme Ave., Philadelphia, PA 19111. Tel.: 215-728-3695; Fax: 215-728-2412; E-mail: EK_Jaffe@fccc.edu.

¶ Present address: 3-Dimensional Pharmaceuticals, Inc., 665 Stockton Dr., Ste. 104, Exton, PA 19341.

** Present address: Novartis Pharma Basel, P.O. Box, Basel 4002, Switzerland.

¹ The abbreviations used are: PBGS, porphobilinogen synthase; ALA, 5-aminolevulinic acid; β ME, 2-mercaptoethanol; 4-OSA, 4-oxosebacic acid; 4,7-DOSA, 4,7-dioxosebacic acid; RMS, root mean-squared; PDB, protein data bank; A-side, acetyl side; P-side, propionyl side.

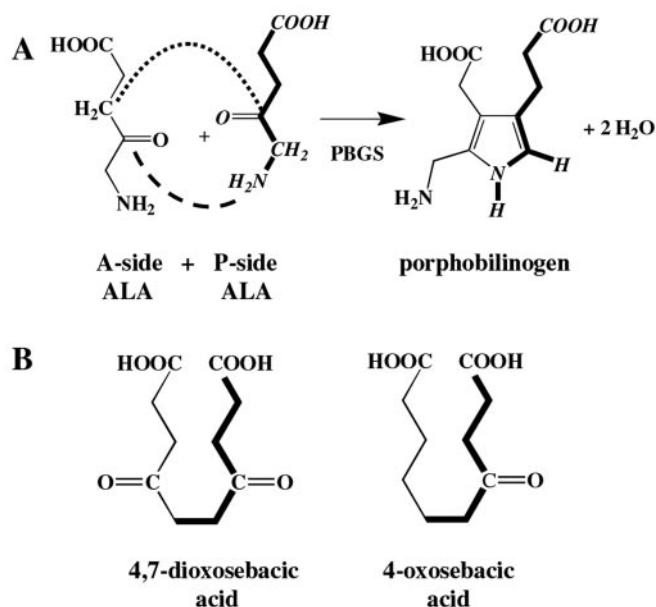


FIG. 1. PBGS-catalyzed reaction and bisubstrate/intermediate site-directed inhibitors. A, PBGS catalyzes the first common step in the biosynthesis of the tetrapyrroles. The chemistry is an asymmetric condensation of two molecules of ALA. A-side ALA contributes the acetyl side chain and retains a free amino group. P-side ALA (*bold bonds, italic*) contributes the propionyl side chain and has its amino group incorporated into the pyrrole ring. B, the PBGS inhibitors 4,7-DOSA and 4-OSA both mimic a putative reaction intermediate wherein C4 of A-side ALA forms a Schiff base with the C5 amino group derived from P-side ALA.

Hs Δ ALK, and HsEclid were assayed in the same fashion as the wild type. To ensure reliable A_{555} values, assays of low specific activity mutants used a 30-min incubation with substrate. Enzyme concentrations were measured with Coomassie Plus protein assay reagent (Pierce) relative to a standard curve prepared with bovine serum albumin.

Inhibition of PBGS by 4-OSA—The five species of PBGS (1 μM subunit) were preincubated under optimal assay conditions for 10 min at 37 $^{\circ}\text{C}$ prior to the addition of 4-OSA over the concentration range of 10 μM to 3 mM; preincubation was allowed to proceed for various times ranging from 90 min to 22 h at 37 $^{\circ}\text{C}$ before initiating the formation of porphobilinogen by addition of ALA-HCl to a final concentration of 10 mM. Porphobilinogen formation was allowed to proceed for 5 min. For *E. coli* PBGS, 4-OSA inhibition data were fitted to the equation $v/v^{\circ} = 1/(1 + (I/IC_{50}))$ (14) using the program SigmaPlot (SPSS[®], Chicago, IL). For other species of PBGS the apparent IC_{50} values for 4-OSA were well above millimolar concentrations and the 10 μM –3 mM inhibition data could not be fit well. In these cases a simple direct comparison of the five species used a 4-OSA concentration of 3 mM and a 24-h enzyme/inhibitor incubation time prior to the addition of ALA.

Crystallization of *E. coli* PBGS Complexed with 4,7-DOSA and 4-OSA and Structure Solution—Crystallizations were carried out with both 4-OSA and 4,7-DOSA as described previously for 4,7-DOSA (3). In both cases, *E. coli* PBGS (9 mg ml⁻¹ in 50 mM Tris-HCl, pH 8.0, 10 mM β ME, 20 μM ZnCl₂, 10 mM MgCl₂) was incubated for 24 h at 37 $^{\circ}\text{C}$ with a 16-fold molar excess of the inhibitor (~4 mM) prior to setting up the crystallization trays. An equal volume of clarified protein was mixed with reservoir buffer containing 1–6% polyethylene glycol 3350, 10% glycerol, 0.1 M Tris-HCl, pH 8.5, and 0.02% sodium azide. The crystals with a diamond-like shape appeared in 1–3 days, and the largest crystals grew to their final size (up to $0.6 \times 0.6 \times 0.3$ mm³) in approximately 2 weeks. Cryoprotection was carried out by transferring a crystal to reservoir solutions containing 17, 23, and 30% glycerol, respectively (3 min in each solution), and the crystal was flash-frozen in a liquid nitrogen vapor. X-ray diffraction data for both complexes were collected from one crystal at 100 K using a QUANTUM-4 CCD detector mounted at synchrotron beamline X9B at Brookhaven National Synchrotron Light Source facility. The data sets consisted of 180 frames chosen to cover at least one asymmetric unit with each frame corresponding to 0.5 $^{\circ}$ oscillation exposed for 35 s. Crystals belong to a tetragonal system, space group, P4₂1₂; unit cell parameters, a = b =

129.0 \AA , and c = 142.8 \AA with two molecules per asymmetric unit. Diffraction intensities were processed with the HKL2000 suite of programs (15), resulting in final data sets with $R_{\text{merge}}(I) = 5.1$ and 5.6% for 126,253 and 92,714 independent reflections and with completeness of 95.7 and 99.8% for the 40–1.7 and 40–1.9 \AA resolution range for 4,7-DOSA and 4-OSA complexes, respectively.

Because the crystals were in both cases isomorphous to that of *E. coli* PBGS complexed with 4,7-DOSA (PDB entry 1I8J), rigid body refinement of the PBGS dimer against the corresponding diffraction data was sufficient to properly orient the protein model in the respective crystal unit cell. Refinement was carried out with program package CNS (16) with weak non-crystallographic symmetry restraints corresponding to weight 25. Model building was performed with program O (17). The final models included one dimer of PBGS molecule complexed with two respective inhibitor molecules, 498 and 433 water molecules for 4,7-DOSA and 4-OSA, respectively, as well as two Zn²⁺ and two Mg²⁺ ions. Five glycerol molecules were found in the 4-OSA structure. The crystallographic *R*-factors were 19.5 and 20.6%, $R_{\text{(free)}}$ parameters were 24.3 and 26.3% for the 1.7- and 1.9- \AA resolution data, and the RMS deviations for bond lengths and bond angles were 0.018 \AA and 1.8 $^{\circ}$ for 4,7-DOSA and 0.019 \AA and 2.0 $^{\circ}$ for 4-OSA, respectively. The coordinates have been deposited in the Protein Data Bank with the PDB codes 1L6S and 1L6Y for immediate release.

RESULTS

Kinetic Evaluation of the Inhibition of PBGS Enzymes by 4-OSA—The inactivation of PBGS by 4,7-DOSA was shown previously to be dependent both upon the concentration of the inhibitor and the preincubation time of the inhibitor and enzyme prior to addition of substrate (3). This is also true for 4-OSA, which was a less potent inactivator than 4,7-DOSA. Fig. 2A illustrates the time and concentration dependence for the interaction of 4-OSA with *E. coli* PBGS using enzyme/inhibitor incubation times of 94 min and 16 h and 4-OSA concentrations from 10 μM to 3 mM. For comparison we also included data from a comparable 100-min incubation of *E. coli* PBGS in which 4,7-DOSA was the inhibitor (3). These data indicate that 4-OSA is far less potent against *E. coli* PBGS than is 4,7-DOSA, consistent with prior reports (6). Using the approximation of Copeland *et al.* (14), the IC_{50} values for *E. coli* PBGS inhibition by 4-OSA at 94 min and 16 h are 0.57 ± 0.06 mM and 0.22 ± 0.01 mM, respectively. The IC_{50} for 4,7-DOSA at 100 min of incubation with *E. coli* PBGS is 0.039 ± 0.002 mM. The reduced sensitivity to 4-OSA relative to 4,7-DOSA is also true for human, *Bradyrhizobium japonicum*, *Pseudomonas aeruginosa*, and *Pisum sativum* (pea) PBGS, where a similar experiment showed marginal if any inactivation by 4-OSA across the range of 10 μM to 3 mM 4-OSA. To compare the five species, Fig. 2B illustrates a 24-h preincubation of 3 mM 4-OSA with all five PBGS and shows a high selectivity for inactivation of *E. coli* PBGS. The control reactions wherein inhibitor was omitted did not lose any significant activity.

Evaluation of 4-OSA with Mutant Forms of Human PBGS—The high selectivity of 4-OSA inactivation for *E. coli* PBGS is in sharp contrast to the species selectivity of inactivation by 4,7-DOSA (3). The latter showed a marked preference for the Zn²⁺-utilizing PBGS and was highly effective against human PBGS, which contains two different types of Zn²⁺ binding sites. In that case, evaluation of an active human PBGS mutant (MinusZnA) that lacked the nonessential Zn²⁺ showed reduced sensitivity to 4,7-DOSA. Of the five species evaluated, only human and *E. coli* PBGS use a catalytic Zn²⁺. Because the number and types of Zn²⁺ sites are a significantly different between human and *E. coli* PBGS, this MinusZnA human PBGS was also evaluated with 4-OSA, and the results are included in Fig. 2C. Consistent with the notion that MinusZnA is more like *E. coli* PBGS, MinusZnA retains only ~65% activity after a 22-h incubation with 3 mM 4-OSA. Thus, MinusZnA is significantly more sensitive to inactivation by 4-OSA than is

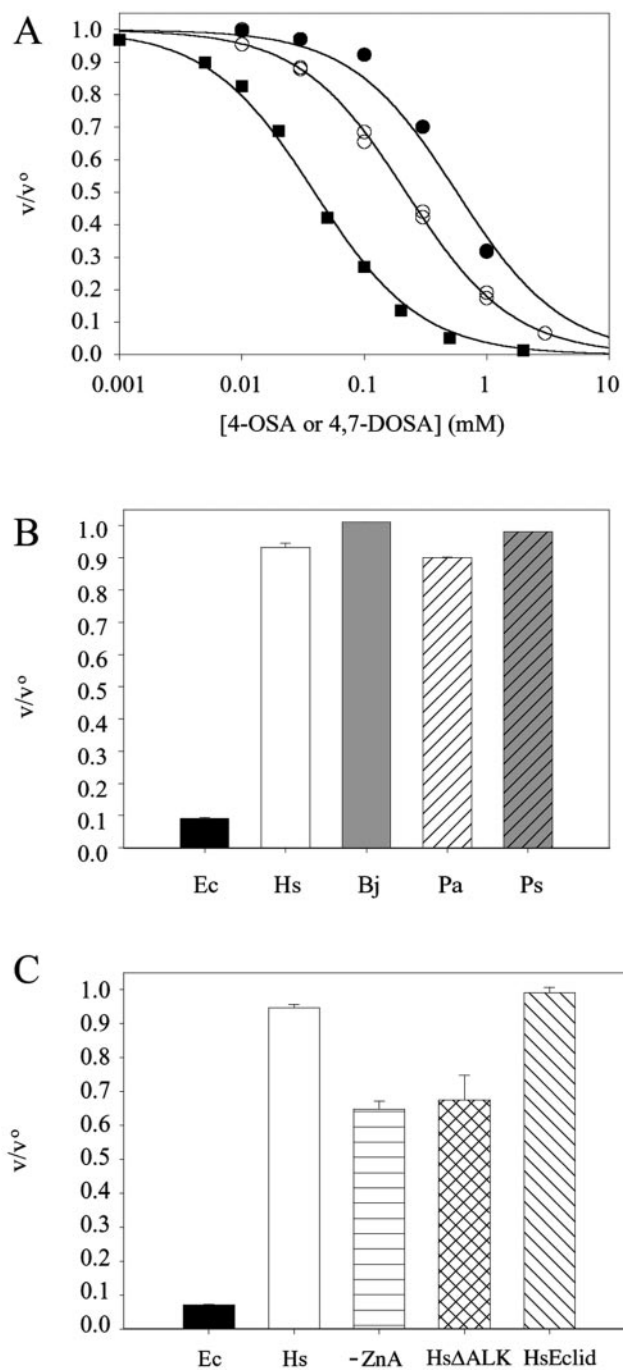


FIG. 2. Inactivation of PBGS by 4-OSA. A, inactivation of *E. coli* PBGS by 4-OSA (circles) relative to previously published data for 4,7-DOSA (squares) (3). Enzyme incubation times (prior to addition of substrate) are 94–100 min for the filled symbols and 16 h for the open symbols. Lines are best fit to the equation $v/v^0 = 1/[1 + ([I]/IC_{50})]$ (14). B, inactivation of a family of wild type PBGS enzymes by 3 mM 4-OSA using a fixed 24-h inhibitor/enzyme incubation time prior to activity assay. The species are *E. coli* (Ec), human (Hs), *B. japonicum* (Bj), *P. aeruginosa* (Pa), and *P. sativum* L. (Ps). For these determinations, the protein concentrations were all at 1 μ M subunit. C, inactivation of mutant or chimeric PBGS by 3 mM 4-OSA using a 24-h enzyme/inhibitor incubation time. The bars correspond to *E. coli* (Ec), human (Hs), human MinusZnA (-ZnA), HsΔALK, and HsEclid.

human PBGS, but it remains far less sensitive than *E. coli* PBGS.

In search for the structural basis for the high selectivity of 4-OSA against *E. coli* PBGS, we compared the known structures (and sequences) of the PBGS to define unique features of

E. coli PBGS. One significant variable feature in the PBGS family of proteins is the length and sequence of the active site lid. Based on the *E. coli* PBGS crystal structure, the lid is defined as the stretch from Ala¹⁹⁶ to Gln²¹⁹. The lid includes all of the residues in this region that are found to be disordered in PBGS structures 1AW5, 1B4K, and 1E51. Fig. 3A shows a structure-based sequence alignment of the active site lid of human, yeast, *E. coli*, *P. aeruginosa*, *B. japonicum*, and *P. sativum* PBGS, which is different from previously published sequence-based alignments. Fig. 3B shows a color-coded structural overlay of the lid region from PBGS corresponding to PDB codes 1E51 (human), 1YLV (yeast), 1I8J (*E. coli*), and 1B4K (*P. aeruginosa*). *E. coli* PBGS is unique among those tested with 4-OSA in that it has the shortest lid sequence. To evaluate the significance of this variable, we created, prepared, and characterized two chimeric “lid-switch” PBGS based on human PBGS using portions of the *E. coli* lid sequence.

The minimal lid switch chimeric protein contains the small portion of the *E. coli* lid that varies in backbone structure. The sequence of this variant, called HsΔALK, is included in Fig. 3A. HsΔALK is an active PBGS with a specific activity of ~4% of wild type human PBGS and a normal K_m value. Purified HsΔALK contains 3.5 Zn²⁺/octamer. As predicted from its increased sequence similarity with *E. coli* PBGS, HsΔALK has increased sensitivity to inhibition by 4-OSA (see Fig. 2C). A less predictable result was observed when a larger portion of the lid sequence was switched. The human PBGS variant HsEclid contains the *E. coli* PBGS lid sequence from Arg²⁰⁴ to Gln²¹⁹ (*E. coli* numbering) as illustrated in Fig. 3A. HsEclid is also an active PBGS with a specific activity of ~12% of wild type human PBGS and a normal K_m value. HsEclid was found to purify with 4.5 Zn²⁺/octamer. Inconsistent with other human PBGS variants that are designed to resemble *E. coli* PBGS, HsEclid is insensitive to inhibition by 4-OSA (see Fig. 2C). The human PBGS variant MinusZnA, whose behavior with 4-OSA is described above, is included in Fig. 3 because one of the mutations (C223A) is in this active site lid region. The Zn²⁺ stoichiometry of HsΔALK and HsEclid suggests that these human PBGS variants retain the property of half-site reactivity, a kinetic property that is well established for human PBGS but not for *E. coli* PBGS.

***E. coli* PBGS Crystal Structures with 4-OSA and 4,7-DOSA**—The PBGS all share a common octameric structure with two monomers forming a dimer around either the non-crystallographic or crystallographic 2-fold symmetry axis and four such dimers forming a PBGS octamer around the 4-fold symmetry axis. Each monomer/subunit forms an $\alpha\beta$ -barrel, the center of which holds the active site residues, while an N-terminal arm that varies in length between species is mutually wrapped around the neighboring subunit forming a compact dimeric structure. The N-terminal arms are involved in extensive subunit interactions within and between dimers. Some PBGS crystal structures show an individual subunit as the asymmetric crystallographic unit, and others (such as those presented here) show a dimer as the asymmetric unit. A variety of data have been interpreted to indicate that an oligomeric structure is required for activity (see Ref. 7). Each active site region is confined to one subunit and isolated from bulk solvent by a lid. The 4,7-DOSA-containing *E. coli* PBGS was the first structure to show that the lid-closed configuration involves extensive hydrogen bonding with the carboxyl group of the A-side ALA molecule, which makes up the acetyl half of porphobilinogen (see Fig. 1A and below) (3). The structure is consistent with the notion that P-side ALA, which makes up the propionyl half of the product, binds first and that the A-side ALA binds second (see Refs. 18 and 19). Similar to other $\alpha\beta$ -

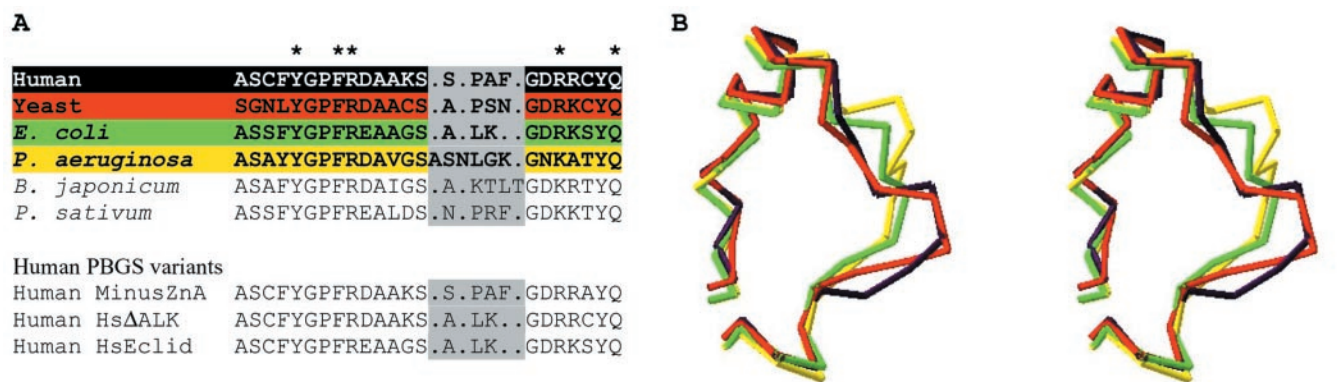


FIG. 3. Variations in the PBGS active site lid. A, structure-based sequence alignment of PBGS from human, yeast, *E. coli*, *P. aeruginosa*, *B. japonicum*, and *P. sativum* L. showing only the active site lid. Sequences are included for the variant and chimeric human PBGS that were evaluated as targets for 4-OSA inhibition. The region containing the R(X)_{10–13}/R/K(X₃)Q sequence forms multiple H-bonding interactions with the carboxyl group derived from A-side ALA. The gray background corresponds to the region of variable sequence length. Sequences in bold are included in and color-coded to the structure alignment in B. Amino acids seen to interact with active site ligands are denoted with an asterisk. B, a stereo view structure alignment showing the closed-lid conformation of human (black), yeast (red), *E. coli* (green), and *P. aeruginosa* (yellow) PBGS for the sequence region shown in A.

barrel enzymes, the ordering and disordering of the active site lid appears to be essential for substrate binding, isolation of the active site from bulk solvent, and product release. The current structures better define these lid motions. The lid residues seen to interact with active site ligands presented here and elsewhere are denoted in Fig. 3.

Here we present the crystal structures of *E. coli* PBGS that has been inactivated by 4-OSA and of another one that has been inactivated by 4,7-DOSA. The latter structure is the same complex that we already published (PDB code 1I8J); however, this time resolution of the diffraction data was extended to 1.7 Å so that we were able to locate 183 extra water molecules, clarify that both Cys^{133A} and Cys^{133B} are adducted with β -mercaptoethanol (see below), and generally provide a more accurate structural description of the protein and the inhibitors. A major new observation based on this structure is a significant variation in the position of the inhibitor half that mimics A-side ALA. Such a result has not been reported for the comparable complex of 4-OSA with yeast PBGS (5). Similar to the complex of 4,7-DOSA-inhibited PBGS, the 4-OSA-inhibited *E. coli* PBGS asymmetric unit contains a dimer, and each subunit of the 4-OSA complex contains one inhibitor molecule, one Zn²⁺ bound at the active site, and one Mg²⁺ bound at the allosteric site (Fig. 4). Unlike the 4,7-DOSA-inhibited PBGS, the 4-OSA complex can form only one Schiff base linkage between each inhibitor and PBGS subunit; this linkage is observed. The RMS deviation between the C α atoms of the two monomers forming a non-crystallographic dimer is 0.25 Å, whereas the RMS deviation between the 4,7-DOSA- and 4-OSA-inhibited PBGS dimers is 0.24 Å. Thus, we conclude that there are no significant differences between the monomers of the dimer or the dimers themselves upon binding either to 4,7-DOSA or 4-OSA (except for part of the lid near Arg²⁰⁴, described below), although the conformations of some side chains (mainly those located on the surface of the octamer) are occasionally different. The average temperature factors are 43.2 and 43.4 Å² for monomers A and B of the 4-OSA-containing complex and 30.2 and 31.2 Å² for monomers A and B of the 4,7-DOSA-containing complex. This indicates that the monomers in each complex have essentially the same degree of flexibility, although the crystals of the 4,7-DOSA complex have better internal order. The symmetry seen in *E. coli* PBGS dimers is in sharp contrast to the high resolution asymmetric dimer seen in *P. aeruginosa* PBGS (PDB code 1B4K) (20) and the less well resolved human PBGS, which contains extensive disorder (PDB code 1E51, unpublished structure).

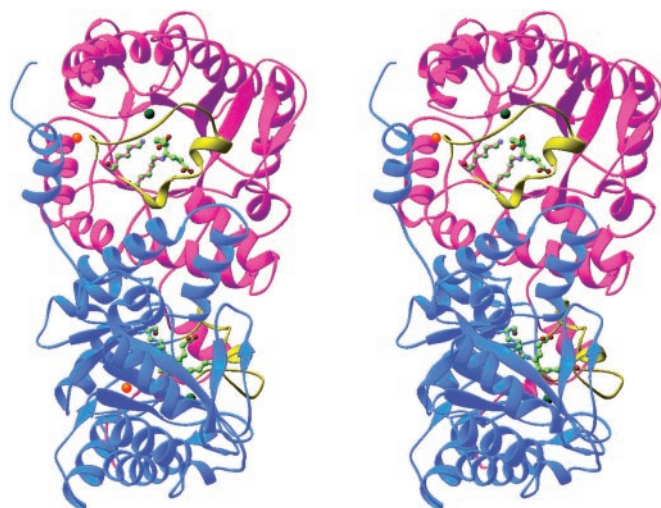


FIG. 4. A stereo diagram of the 4-OSA inactivated *E. coli* PBGS dimer. The two monomers are shown in blue and magenta, Zn²⁺ is dark green, Mg²⁺ is orange, and the active site lid is yellow. The two active site lysine residues are shown (ball-and-stick) with bonds colored according to the subunit; Lys²⁴⁶ makes Schiff base to atom C4 of the inhibitor. The 4-OSA molecules are shown (ball-and-stick) with bonds in green. Atom color code is C, green; N, blue; O, red.

The two *E. coli* PBGS structures presented here clarify the amino acid identity of position 133, which had previously been identified as a lysine (2). The DNA sequence indicates Cys¹³³ and mass spectroscopy analysis of an AspN digest was obtained herein to demonstrate the existence of a cysteine in this position. Because Cys¹³³ is located on the surface of the protein, which has been purified and stored in the presence of mercaptoethanol, this residue appears as an adduct of β ME and cysteine (*S,S*-2-(hydroxyethyl)thiocysteine). The adduct was first reported in a V23C variant of staphylococcal nuclease (21), and the current electron density is an excellent fit to this model.

Mechanism of Inhibition by 4-OSA and 4,7-DOSA—The inhibitor molecules are clearly seen in the difference electron density maps in the area of the active site next to Lys¹⁹⁴ and Lys²⁴⁶ in both monomers. In the case of 4,7-DOSA there are two covalent linkages between the protein and the inhibitor, and in the case of 4-OSA there is one covalent linkage. Fig. 5A illustrates an electron density map of 4-OSA bound to the enzyme, and Fig. 5B shows a comparison between the 4-OSA- and 4,7-DOSA-inhibited proteins. In both cases C1-C5 of the

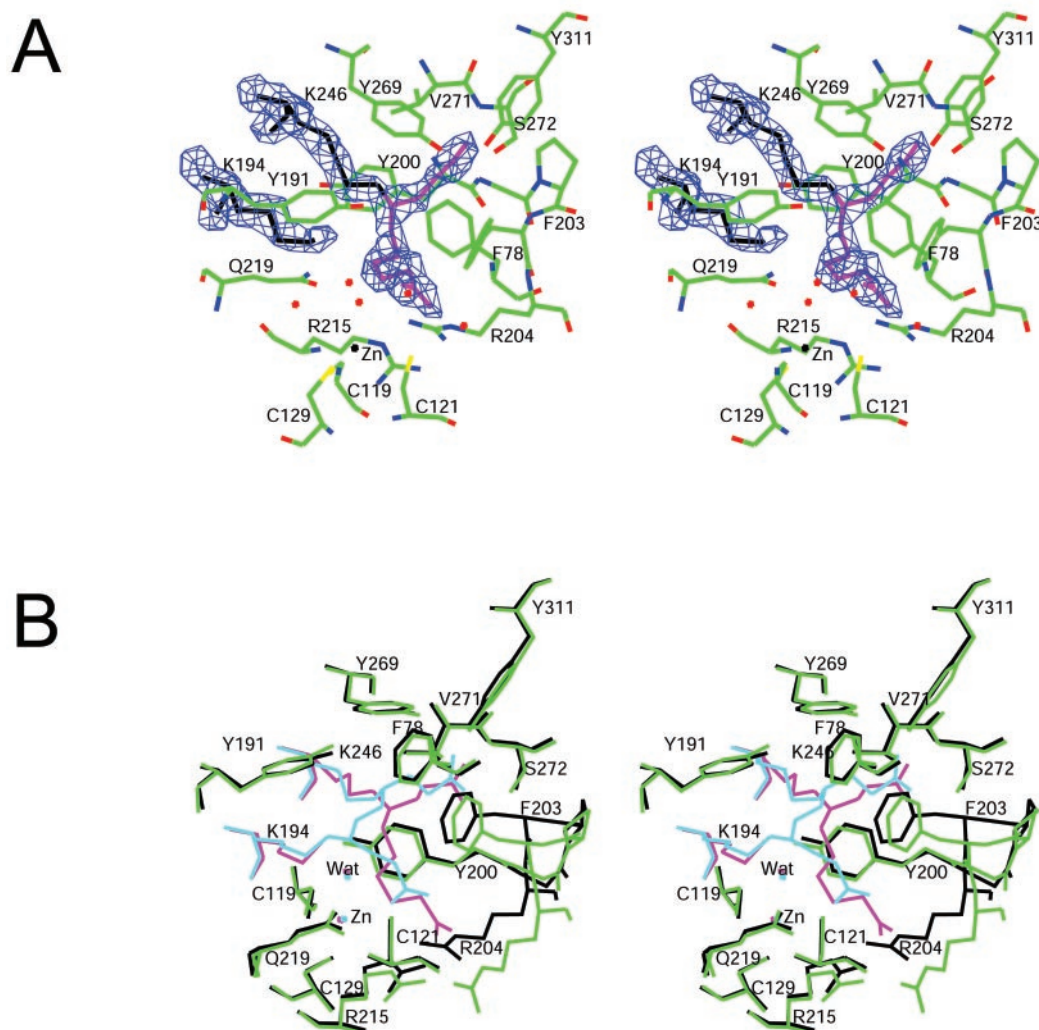


FIG. 5. **The active sites of 4-OSA and 4,7-DOSA inactivated *E. coli* PBGS.** A, stereo picture of the electron density corresponding to 4-OSA, Lys¹⁹⁴, and Lys²⁴⁶ at the active site of the enzyme. Atoms derived from 4-OSA are in magenta; atoms of Lys¹⁹⁴ and Lys²⁴⁶ are black; carbons from protein are green; nitrogen is blue; oxygen is red; sulfur is yellow; and Zn²⁺ is black. Highly conserved active site water molecules are included. The illustration shows a $2F_o - F_c$ difference electron density map contoured at a level of 1.5σ . B, stereo overlay of 4,7-DOSA (blue)-inhibited *E. coli* PBGS (black) with 4-OSA (magenta)-inhibited *E. coli* PBGS (green).

inhibitor are bound with a Schiff base linkage between C4 and the ϵ -amino group of Lys²⁴⁶. In these cases, as well as in related PBGS structures with inhibitors bound in the P-side ALA binding pocket (PDB codes: 1B4E, 1B4K, 1EB3, 1YLV, 1I8J, 1GJP, 1H7N, 1H7P, 1H7R), the C1 carboxyl oxygens of the inhibitor make hydrogen bonds with Ser²⁷² and Tyr³¹¹. The positions of the C2 and C3 atoms of each inhibitor are well defined but not equivalent to each other. The variation in these positions mimics the reported alternate conformations of levulinic acid bound as the P-side Schiff base to yeast PBGS (PDB code 1H7N) (22). This variation defines the limited spatial flexibility of P-side ALA and dictates that these atoms cannot reorient much in response to required hybridization changes at C4. The position of C1-C4 of 4-OSA more closely resembles that of the product porphobilinogen. As reported previously for the 1.9-Å structure of 4,7-DOSA-inhibited *E. coli* PBGS, the bond between C5 and C6 of the inhibitor has a distorted cis-configuration (torsion angle of C4-C5-C6-C7 is $\sim 65^\circ$) to accommodate a second Schiff base linkage between C7 and the ϵ -amino group of Lys¹⁹⁴. Because there is no Schiff base to Lys¹⁹⁴ in the 4-OSA-inhibited enzyme, the conformation around the C5-C6 bond (torsion angle C4-C5-C6-C7 is $\sim -88^\circ$) and the positions of C5-C10 of reacted 4-OSA are significantly different from those

seen for 4,7-DOSA (Fig. 5B). This suggests that A-side ALA has much greater positional flexibility than does P-side ALA. Positional flexibility is essential to accommodate the multiple hybridization changes required in the formation of porphobilinogen. In the case of both inhibitors, the A-side ALA half (C8-C10) extends out toward the lid where it makes extensive hydrogen-bond linkages between the C10 carboxyl oxygens and arginine residue(s). However, the hydrogen-bonding pattern is not the same for the two inhibitors, as illustrated schematically in Fig. 6. Unlike 4,7-DOSA, 4-OSA does not interact with Gln²¹⁹ through hydrogen bonds directly; instead it does so through a bridging water molecule. This is the same water molecule that forms similar bridging hydrogen bonds between Gln²¹⁹ and Arg²⁰⁴ in the 4,7-DOSA-containing complex. To accommodate the different structure of the A-side half of the 4-OSA inhibitor, the side chain of Arg²⁰⁴ moves approximately 2.5 Å away from the position it occupied in the 4,7-DOSA complex (Fig. 5B) and is locked in this new position by a hydrogen bond between its side chain NH1 atom and the carbonyl oxygen of Gly²¹³. The position of Arg²⁰⁴ in the absence of an A-side ligand (structure 1B4E) is much like that of the 4,7-DOSA-containing complex, but its H-bonds are strictly to water. Despite the different position of the Arg²⁰⁴ side chain in

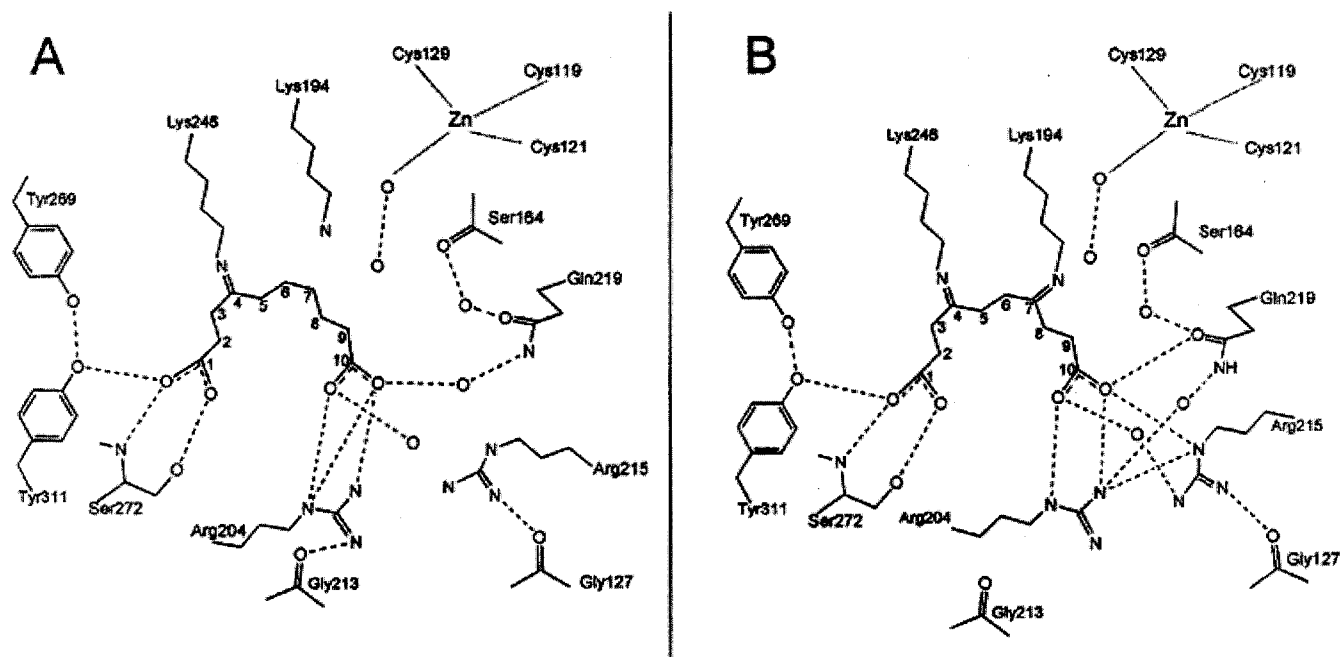


FIG. 6. Schematic diagram of the hydrogen bonding of 4-OSA (A) and 4,7-DOSA (B) with *E. coli* PBGS. The carbon atoms of 4-OSA and 4,7-DOSA are numbered. Water molecules are represented by single oxygen atoms as O. Dashed lines indicate potential hydrogen bonds using a heteroatom distance of ≤ 3.2 Å. Hydrogen bonds are depicted for subunits A. In subunit B the Gly²¹³(O)-Arg²⁰⁴(N), the 4-OSA(O)-Arg²⁰⁴(NE), and the 4-OSA(O)-water (connected to Gln²¹⁹) distances are 3.5–3.8 Å. Dotted lines indicate the Zn²⁺ ligand bonds, which are each ~ 2.4 Å.

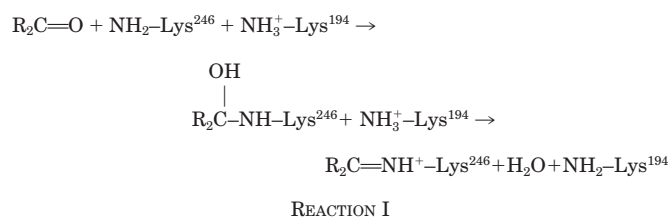
these structures, the C α atoms of this part of the lid (positions 203–205) move <1.4 Å. The difference in the position and conformation of the A-side of 4-OSA results in C7 being approximately 1 Å closer to the catalytic Zn²⁺; the distance C7-Zn²⁺ is 4.5 versus 5.5 Å in 4,7-DOSA. There are several ordered water molecules found within a 5-Å distance from the inhibitor in the A-side of both complexes that are included in Fig. 5. They are all the same in both structures and are also seen in high resolution structures of yeast PBGS and *P. aeruginosa* PBGS.

DISCUSSION

4-OSA Bound to PBGS—The structures presented in Fig. 5B can be compared with recently published crystal structures of these inhibitors with yeast PBGS (PDB codes 1EB3 and 1GJP) (5). In these structures the A-side of the inhibitor is modeled such that the carboxyl groups of 4-OSA and 4,7-DOSA are in nearly the same position as each other. In the case of 4-OSA, we consider this interpretation questionable because Arg²²⁰ (the counterpart of *E. coli* Arg²⁰⁴) is shifted 2.6 Å away from the active site in a manner similar to what is found in the *E. coli* 4-OSA-inhibited PBGS structure. In the yeast structure, the dramatically shifted Arg²²⁰ does not interact with the inhibitor or any other atoms except for two water molecules on the surface of the protein. In fact, 4-OSA of 1GJP is reported as “somewhat disordered,” and the presented electron density map is completely lacking density for one of the A-site carboxyl oxygens. A more compelling reason to question the model for 4-OSA bound to yeast PBGS comes from a comparison of the yeast PBGS structure 1GJP with the *E. coli* PBGS complex presented here. When one superimposes the 4-OSA-inhibited *E. coli* PBGS structure (where inhibitor was perfectly ordered) with 1GJP (superposition was based only on the protein parts of the complex), we find that our 4-OSA inhibitor makes exactly the same hydrogen bonds with the yeast enzyme, including Arg²²⁰ in its new position, as in *E. coli* 4-OSA PBGS complex. In other words, the structure of 4-OSA as it is found in the complex with *E. coli* PBGS is energetically more favorable upon binding to the yeast enzyme than the one that was reported in

the crystal structure of the complex of 4-OSA with yeast PBGS itself (5). Taken together, these points shed doubt on the interpretation of the conformation of 4-OSA bound to yeast PBGS in structure 1GJP.

The PBGS-catalyzed Reaction Mechanism, Active Site Lid Motion, and Enzyme-bound Active Site Water—The PBGS-catalyzed reaction is illustrated in Fig. 1. The first ALA to bind to PBGS is P-side ALA (18). P-side ALA forms a Schiff base intermediate to an active site lysine (Lys²⁴⁶ in *E. coli* PBGS) (23). Metals are not required for the binding or reactivity of P-side ALA (19). Maintenance of the deprotonated Schiff base-forming lysine is accomplished by the neighboring basic residue (here Lys¹⁹⁴). As with all Schiff base-forming enzymes, one expects to be able to identify the residue that serves in the removal of the oxygen atom from the carbinolamine intermediate that precedes P-side Schiff base formation. This residue is not apparent in any PBGS crystal structures and has not been addressed in prior publications. The existing PBGS structures all place the P-side Schiff base in a very hydrophobic environment, part of which is composed of aromatic residues in the N-terminal portion of the active site lid (see Fig. 5). Because this Schiff base occurs for both 4-OSA and 4,7-DOSA, and the resulting water molecule is not observed near the P-side of the inhibitor, we conclude that this first water molecule must relocate prior to lid closure. One possible acceptor for the carbinolamine hydroxyl group would be the protonated Lys¹⁹⁴ in a rotamer conformation different from that which is observed in here. In this case the reaction would be as shown in Reaction I.



Alternatively, one may propose that the protonated base that dehydrates the P-side carbinolamine comes from an alternate configuration of the active site lid. The lid contains many conserved basic residues (see Fig. 3), which (as seen in the structures presented here) can interact with the A-side carboxyl group later in the reaction but may serve an additional function earlier.

The second ALA to bind to PBGS is A-side ALA. For those PBGS that use a catalytic Zn^{2+} , the metal ion is required for A-side ALA binding and reactivity (19). The crystal structures of 4,7-DOSA- and 4-OSA-inhibited PBGS support the mechanistic hypothesis that the keto oxygen removed from C4 of A-side ALA (C7 of the inhibitors) ends up coordinated to the catalytic Zn^{2+} (3). We have proposed that A-side ALA binds as a bidentate Zn^{2+} ligand through the C4 keto oxygen and the C5 amino group (24). Molecular modeling studies indicate that this complex fits into the A-side ALA binding pocket and takes advantage of the unique flexibility of Zn^{2+} to accommodate various coordination numbers and geometries (25). The coordination environment of this Zn^{2+} is unusual for a catalytic Zn^{2+} in that it contains three cysteine ligands that derive from a short stretch of 11 amino acids. The structures presented here indicate that the Zn^{2+} -bound water molecule is appropriately positioned to have derived from the keto group analogous to that of A-side ALA.

Based on the extensive hydrogen-bonding interactions between the A-side carboxylic acid group of 4-OSA and 4,7-DOSA and the active site lid residues, we conclude that A-side ALA binding necessitates the ordering or reordering of the active site lid. Comparison of the conformation of the lid between the 4,7-DOSA, 4-OSA, and 1B4E (the complex of *E. coli* PBGS and levulinic acid) structures shows that most of the conformational change upon inhibitor binding occurs in the part of the lid between positions 200 and 205. The deviation of the $C\alpha$ atoms in this region does not exceed 1.4 Å, the side chain of Arg²⁰⁴ is shifted approximately 2.5 Å away from the active site to accommodate the A-side part of 4-OSA, and the other side chains occupy very much the same positions in all three complexes.

The PBGS-catalyzed reaction involves significant hybridization changes at multiple carbon centers (see Fig. 1). As described above, large translational motion is not possible for the propionyl side chain of P-side ALA. For A-side ALA, the C5 amino-containing portion appears relatively fixed through interaction with the catalytic Zn^{2+} . This is apparent from prior ¹³C and ¹⁵N NMR data (26) and from the observation that the amino group of the product porphobilinogen is chelated to the Zn^{2+} in the unpublished human PBGS structure 1E51 and in the complex of *E. coli* PBGS with porphobilinogen.² Thus, to accommodate the significant hybridization changes, particularly at C3 of A-side ALA, the acetyl side chain must experience substantial mobility throughout the course of the reaction. One significant contribution of the current structure is the visualization of a different orientation for the inhibitor atoms C6–C10 analogous to C1–C5 of the A-side ALA. We propose that the observed multiple hydrogen bonds between the C10 carboxyl and Arg²⁰⁴, Arg²¹⁵, Gln²¹⁹, and associated water molecules change conformation to accommodate various positions of C1 and C2 of A-side ALA during the course of the PBGS-catalyzed reaction.

A particularly vexing question in understanding the PBGS-catalyzed reaction mechanism has been the identification of the residues that serve as acceptors for the four protons and two oxygen atoms lost in the condensation of two ALA molecules to

porphobilinogen. The contribution of these crystal structures to identifying the oxygen acceptors is discussed above. The proton acceptor(s) for the deprotonations of the amino group and C5 of P-side ALA appear to be the two active site lysine residues as discussed previously (2). Remarkably, there are no amino acids positioned to be the proton acceptors at A-side ALA. Rather, comparison of these and other PBGS structures shows a bath of highly conserved water molecules adjacent to and including the Zn^{2+} -bound water that initially derives from C4 of A-side ALA. These water molecules are illustrated in Fig. 5A. Their positions are highly conserved, and they are isolated from bulk solvent. These water molecules appear to be the only possible acceptors for the protons that must be lost from A-side ALA. The implication of water as the proton acceptor in the formation of an enamine from an imine, akin to the removal of the first proton from C3 of A-side ALA, is not without precedent. Analogous chemistry has recently been implicated in the mechanism of D-2-deoxyribose-5-phosphate aldolase (27).

In summary, the PBGS-catalyzed reaction mechanism has been a subject of debate for more than three decades. In fact, many different detailed reaction mechanisms have been illustrated in the literature (*e.g.* Refs. 2, 4–6, 18, 28–30), most of which do not include a role for one or more essential metal ions. Basic features such as the order of bond-making and bond-breaking reactions in the PBGS-catalyzed reaction remains uncertain and may not be conserved for all of the PBGS from different species. The current structures do not resolve these uncertainties. However, the new structures of 4-OSA- and 4,7-DOSA-inhibited PBGS help identify the acceptor groups for the atoms that are abstracted from the substrate molecules. They suggest that enzyme-bound active site water molecules play pivotal roles in the PBGS-catalyzed reaction and that there is a mechanistic importance to fluctuations between multiple conformations of the active site lid.

Acknowledgments—We thank Drs. Nicole Frankenberg, Robert Petrovich, and Laura Mitchell for essential roles in purifying some of the PBGS enzymes studied, Dr. Steven Seeholzer of the Biochemistry and Biotechnology Facility for carrying out the mass spectral analyses, and Professor Karen Allen of Boston University for helpful discussions.

REFERENCES

- Jaffe, E. K. (2000) *Acta Crystallogr. Sect. D* **56**, 115–128
- Erskine, P. T., Norton, E., Cooper, J. B., Lambert, R., Coker, A., Lewis, G., Spencer, P., Sarwar, M., Wood, S. P., Warren, M. J., and Shoolingin-Jordan, P. M. (1999) *Biochemistry* **38**, 4266–4276
- Kervinen, J., Jaffe, E. K., Stauffer, F., Neier, R., Wlodawer, A., and Zdanov, A. (2001) *Biochemistry* **40**, 8227–8236
- Stauffer, F., Zizzari, E., Soldermann-Pissot, C., Faurite, J.-P., and Neier, R. (2001) *Chimia* **55**, 314–319
- Erskine, P. T., Coates, L., Newbold, R., Brindley, A. A., Stauffer, F., Wood, S. P., Warren, M. J., Cooper, J. B., Shoolingin-Jordan, P. M., and Neier, R. (2001) *FEBS Lett.* **503**, 196–200
- Jarret, C., Stauffer, F., Henz, M. E., Marty, M., Luond, R. M., Bobalova, J., Schurmann, P., and Neier, R. (2000) *Chem. Biol.* **7**, 185–196
- Kervinen, J., Dunbrack, R. L., Jr., Litwin, S., Martins, J., Scarrow, R. C., Volin, M., Yeung, A. T., Yoon, E., and Jaffe, E. K. (2000) *Biochemistry* **39**, 9018–9029
- Petrovich, R. M., Litwin, S., and Jaffe, E. K. (1996) *J. Biol. Chem.* **271**, 8692–8699
- Frankenberg, N., Heinz, D. W., and Jahn, D. (1999) *Biochemistry* **38**, 13968–13975
- Jaffe, E. K., Volin, M., Bronson-Mullins, C. R., Dunbrack, R. L., Jr., Kervinen, J., Martins, J., Quinlan, J. F., Jr., Sazinsky, M. H., Steinhilber, E. M., and Yeung, A. T. (2000) *J. Biol. Chem.* **275**, 2619–2626
- Mitchell, L. W., and Jaffe, E. K. (1993) *Arch. Biochem. Biophys.* **300**, 169–177
- Frankenberg, N., Jahn, D., and Jaffe, E. K. (1999) *Biochemistry* **38**, 13976–13982
- Jaffe, E. K., Martins, J., Li, J., Kervinen, J., and Dunbrack, R. L., Jr. (2001) *J. Biol. Chem.* **276**, 1531–1537
- Copeland, R., Lombardo, D., Giannaras, J., and Decicco, C. (1995) *Bioorg. Med. Chem. Lett.* **5**, 1947–1952
- Otwinowski, Z., and Minor, W. (1997) *Methods Enzymol.* **276**, 307–326
- Brunger, A. T., Adams, P. D., Clore, G. M., DeLano, W. L., Gros, P., Grosse-Kunstleve, R. W., Jiang, J.-S., Kuszewski, J., Nilges, M., Pannu, N. S., Read, R. J., Rice, L. M., Simonson, T., and Warren, G. L. (1998) *Acta Crystallogr. Sect. D* **54**, 905–921
- Jones, T. A., Zou, J. Y., Cowan, S., and Kjeldgaard, M. (1991) *Acta Crystallogr. Sect. A* **47**, 110–119

² H. L. Carrell, personal communication.

18. Jordan, P. M., and Seehra, J. S. (1980) *J. Chem. Soc. Chem. Commun.* **5**, 240–242
19. Jaffe, E. K., and Hanes, D. (1986) *J. Biol. Chem.* **261**, 9348–9353
20. Frankenberg, N., Erskine, P. T., Cooper, J. B., Shoolingin-Jordan, P. M., Jahn, D., and Heinz, D. W. (1999) *J. Mol. Biol.* **289**, 591–602
21. Wynn, R., Harkins, P. C., Richards, F. M., and Fox, R. O. (1996) *Protein Sci.* **5**, 1026–1031
22. Erskine, P. T., Newbold, R., Brindley, A. A., Wood, S. P., Shoolingin-Jordan, P. M., Warren, M. J., and Cooper, J. B. (2001) *J. Mol. Biol.* **312**, 133–141
23. Spencer, P., and Jordan, P. M. (1995) *Biochem. J.* **305**, 151–158
24. Jaffe, E. K. (1995) *J. Bioenerg. Biomembr.* **27**, 169–179
25. Bock, C. W., Katz, A. K., Markham, G. D., and Glusker, J. P. (1999) *J. Am. Chem. Soc.* **121**, 7360–7372
26. Jaffe, E. K., Markham, G. D., and Rajagopalan, J. S. (1990) *Biochemistry* **29**, 8345–8350
27. Heine, A., DeSantis, G., Luz, J. G., Mitchell, M., Wong, C.-H., and Wilson, I. A. (2001) *Science* **294**, 369–374
28. Nandi, D. L., and Shemin, D. (1968) *J. Biol. Chem.* **243**, 1236–1242
29. Barnard, G. F., Itoh, R., Hohberger, L. H., and Shemin, D. (1977) *J. Biol. Chem.* **252**, 8965–8974
30. Neier, R. (1996) *Advances in Nitrogen Heterocycles*, Vol. 2, pp. 35–146, JAI Press, Greenwich, CT